**P6.10** DIURNAL, SEASONAL, AND INTERANNUAL VARIATIONS OF CLOUD PROPERTIES DERIVED FOR CERES FROM IMAGER DATA

Patrick Minnis, David F. Young
Atmospheric Sciences, NASA Langley Research Center, Hampton, VA 23681

Sunny Sun-Mack, Qing Z. Trepte, Yan Chen, Richard R. Brown, Sharon Gibson
SAIC, Hampton, VA 23666

Patrick W. Heck
CIMSS, University of Wisconsin-Madison, Madison, WI, USA

## 1. INTRODUCTION

Simultaneous measurement of the radiation and cloud fields on a global basis is a key component in the effort to understand and model the interaction between clouds and radiation at the top of the atmosphere, at the surface, and within the atmosphere. The NASA Clouds and Earth's Radiant Energy System (CERES) Project, begun in 1998, is meeting this need (Wielicki et al. 1998). Broadband shortwave (SW) and longwave radiance measurements taken by the CERES scanners at resolutions between 10 and 20 km on the Tropical Rainfall Measuring Mission (TRMM), *Terra*, and *Aqua* satellites are matched to simultaneous retrievals of cloud height, phase, particle size, water path, and optical depth *OD* from the TRMM Visible Infrared Scanner (VIRS) and the Moderate Resolution Imaging Spectroradiometer (MODIS) on *Terra* and *Aqua*. Besides aiding the interpretation of the broadband radiances, the CERES cloud properties are valuable for understanding cloud variations at a variety of scales. In this paper, the resulting CERES cloud data taken to date are averaged at several temporal scales to examine the temporal and spatial variability of the cloud properties on a global scale at a 1° resolution.

In earlier studies (Minnis et al. 2002, 2003), it was demonstrated that the CERES cloud property retrievals from *Terra* MODIS, *Aqua* MODIS, and TRMM VIRS were very consistent with the most significant difference being the retrieval of smaller cloud droplet effective radii $r_e$ from the *Terra* data. Comparisons of other parameters with climatological data also showed that the cloud amounts from both TRMM and *Terra* were in good agreement with the zonal means from long-term surface observations and were typically 0.07 - 0.08 less than those from the International Satellite Cloud Climatology Project (ISCCP) dataset (Rossow and Schiffer, 1999) over the Tropics. Comparisons with surface-based retrievals showed that the mean CERES-derived cloud *OD*s for stratus clouds were within 6% of their surface counterparts. These cloud properties have been already been responsible for dramatically improving estimates of the Earth's radiation budget (ERB) by facilitating the most accurate representation of the anisotropy of the radiance fields leaving the Earth-atmosphere system (Loeb at al. 2003). They will also be valuable for linking the hydrological cycle and ERB and for improving climate model processes. The importance of measuring cloud and radiation changes simultaneously has recently been highlighted by measurements of Earth shine that were used to infer a 5 $Wm^{-2}$ increase in the SW flux reflected from the Earth between 2000 and 2003 (Palle et al. 2004). Changes of that magnitude are comparable to those from a major volcanic eruption and should be apparent in the CERES cloud and radiation record and as well as in other measures of the state of the climate.

*Corresponding author address: Patrick Minnis, NASA Langley Research Center, MS 420, Hampton, VA 23681-2199. email: p.minnis@nasa.gov.

## 2. DATA & METHODOLOGY

The TRMM VIRS has provided coverage at all local hours between 37°N and 37°S every 46 days since January 1998. VIRS 2-km data were analyzed through July 2001 to produce a TRMM Edition 2 cloud property Single Scanner Footprint (SSF) dataset. *Terra* and *Aqua* MODIS data, hereafter, simply *Terra* and *Aqua*, have been taken since February 2000 and July 2002, respectively. At the time of this writing, *Terra* data have been analyzed to produce the CERES *Terra* Edition 2a SSF dataset through January 2004. Every other 1-km MODIS pixel and every fourth scan line are sampled to minimize processing time and data storage. The CERES *Aqua* Edition 1 SSF dataset is currently being generated. The SSF consists of the cloud properties, imager radiances, and other parameters convolved with the CERES scanner point spread function into the each CERES footprint to effect an optimal match between the cloud and radiation parameters. The CERES fluxes are available on the VIRS SSFs only from January -August 1998 and during March 2000 because of a CERES scanner failure.

To create the cloud datasets, each imager pixel is initially classified as clear or cloudy using updated versions of the CERES classification schemes that employ the 0.64 (visible), 1.6 or 2.1 (near infrared), 3.7 (solar infrared), 10.8 (infrared), and 12 (split window) $\mu$m radiances (Trepte et al., 1999, 2002). The 1.6-$\mu$m channel is used as the near-infrared data from VIRS

and *Terra*, while the 2.1-$\mu$m channel is used for *Aqua* because of problems with the *Aqua* 1.6-$\mu$m channel. The radiances are compared with predicted clear-sky radiances based on empirical estimates of spectral clear-sky albedo (Sun-Mack et al., 1999, 2003) and on skin temperatures from the CERES Meteorology, Ozone, and Aerosol (MOA) dataset adjusted using empirical estimates of spectral surface emissivity (Chen et al., 2002) and atmospheric absorption calculated with the MOA vertical profiles of temperature and humidity. The CERES MOA profiles are based on the European Center for Medium-range Weather Forecasting (ECMWF) reanalyses for VIRS and on the Global Modeling Assimilation Office GEOS 4.03 (DAO, 1997) reanalyses for *Terra* Edition 2a and *Aqua* Edition 1. The differences between the 1.6- and 2.1-$\mu$m reflectances for clear snow surfaces necessitated some adjustments to the cloud mask algorithms that are described by Minnis et al. (2003).

One of three different techniques is used to derive cloud temperature $T_c$, height $z_c$, thickness, phase, effective droplet radius $r_e$ or effective ice crystal diameter $D_e$, *OD*, and water path *WP* from these same radiances for each cloudy pixel. The visible infrared solar-infrared split-window technique (VISST), an updated version of the 3-channel daytime method of Minnis et al. (1995), is used during daytime, which is defined as the time when the solar zenith angle *SZA* is less than 82°. At other times of day, the solar-infrared infrared split-window technique (SIST) is used to determine all of the parameters. The SIST, an improved version of the 3-channel nighttime method of Minnis et al. (1995), only uses thermal and solar infrared data. Thus, its retrievals are valid only for optically thin clouds. When the SIST is used, default values are used for all parameters except phase, $T_c$, and $z_c$ for clouds with *OD* < 8. The third method, developed by Platnick et al. (2001), is designated the solar-infrared infrared near-infrared technique (SINT) and is only applied to MODIS data during the daytime for clouds over snow or ice backgrounds. The 2.13-$\mu$m channel on *Aqua* is used instead of the 1.6-$\mu$m channel in the SINT. Determination of the background surface as snow or ice can either come from the scene classification for adjacent clear pixels or from the snow and ice maps used in the CERES data stream (Trepte et al., 2002). All of the methods compute both ice and liquid water solutions that simultaneously determine $T_c$, *OD*, and particle size. Each method iteratively matches the observed radiances to TOA radiances calculated using emittance and reflectance parameterizations that account for atmospheric attenuation and surface reflectance and emission. The cloud reflectances and emittances are included in the parameterizations (Minnis et al., 1998, Arduini et al., 2002) using updated lookup tables for each specific channel. The phase is selected for each pixel based on the cloud temperatures, the availability of a solution, best consistency with a solution, and the altitude of the cloud.

The pixel-level data are convolved with the individual broadband CERES radiative fluxes to provide the link between clouds and the radiation budget. These SSF products include the cloud fraction and mean associated properties for up to two cloud layers. No cloud properties could be retrieved for ~6.7% of pixels classified as cloudy during the daytime. At night, only 1.4% of the cloudy pixels are inconsistent with the parameterizations. Most of the no-retrieval pixels occur in polar regions over snow-covered surfaces or over very bright deserts. In the former instance, the SINT is unable to find a match, probably because of uncertainties in the clear-sky reflectance fields. In the latter case, the pixels detected as clouds may actually be heavy concentrations of aerosols that are misclassified as clouds. Over most ocean and land areas outside the polar regions and Saharan Desert, the no-retrievals account for 1 - 2% of the total number of cloudy pixels. To account for the no-retrievals, the SSF convolution assigns the mean cloud properties from cloudy pixels in the footprint with retrieved values to the no-retrieval pixels, if more than 1/9 of pixels in the footprint have valid cloud retrievals. Otherwise, only the valid cloudy pixels are used and the no-retrieval pixels are not considered as part of the total number of pixels in the footprint.

Edition-2 VIRS cloud products are currently available for January 1998 - July 2001, but the CERES fluxes are only available for January - August 1998 and March 2000. As of this writing, the CERES Edition-2 *Terra* cloud properties have been completed for the period February 2000 through January 2004. Edition-1 *Aqua* products have been produced for July 2002 - October 2002. *Terra* and *Aqua* analyses are ongoing.

## 3. RESULTS AND DISCUSSION

The 4-year mean seasonal total cloud amounts *Ac* from *Terra* are plotted in Fig. 1 as a function of latitude. These results represent the combination of daytime and nighttime retrievals. The seasons are defined relative to the Northern Hemisphere with winter defined by December, January, and February. The seasonal variation in zonal mean *Ac* is greatest over the polar regions and almost non-existent between 45°S and 60°S. The movement of Intertropical Convergence Zone (ITCZ) is evident in the shift in the relative tropical maximum from 10°N during the summer and fall to 10°S in winter. The annual mean cloud amounts computed from the seasonal averages are plotted in Fig. 2 with the zonal mean cloud amounts derived from all available surface observations for the 1971-1996 period and with zonal averages from ISCCP for 1983-2001. The CERES *Terra* MODIS total cloud amounts track the surface values except in the Arctic where the CERES values are 5 - 17% less than the surface means. Other large differences are evident near the South Pole. The surface means are slightly larger than their CERES counterparts in the Tropics and northward of 55°N.

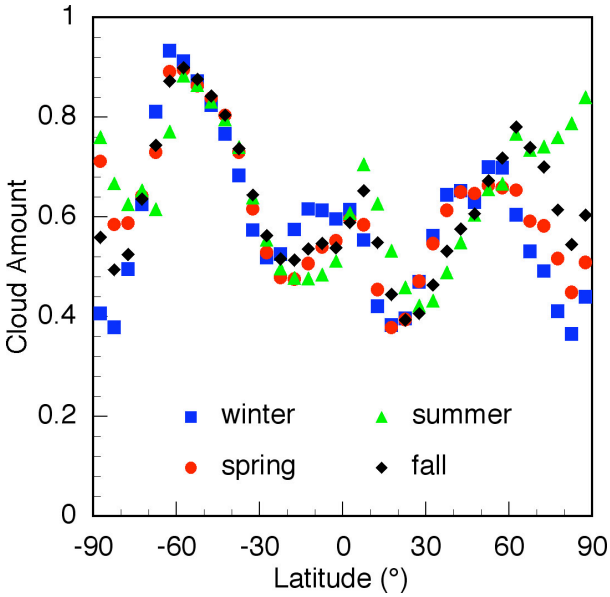


*Fig. 1. Mean seasonal total cloud cover from CERES Terra MODIS analyses, 2000-2003.*

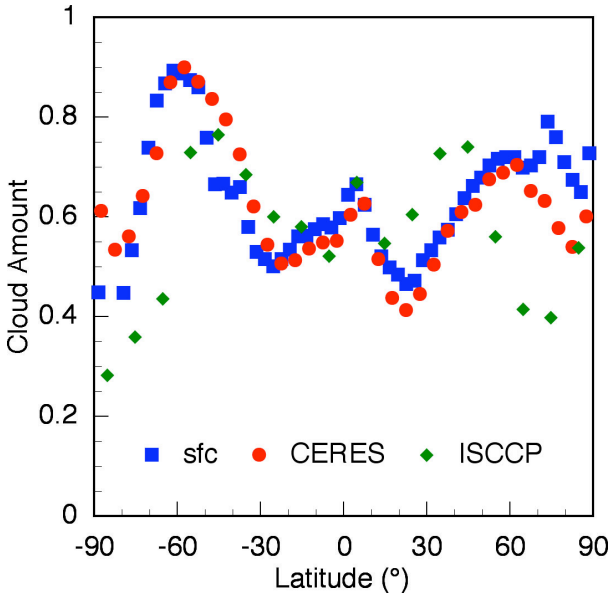


*Fig. 2. Mean total cloud cover from surface (sfc) observations (1971-1996), CERES Terra MODIS (2000-2003), and ISCCP (1983-2001).*

The CERES averages are slightly larger in the southern midlatitudes and over the South Pole. The ISCCP values are the greatest of the three datasets between 30°S and 40°N and much smaller than either dataset poleward of the 50° latitudes. Despite substantial zonal differences between the three datasets, the annual mean global cloud cover from the surface, CERES, and ISCCP, are remarkably close with values of 0.609, 0.602, and 0.604, respectively.

The large differences between CERES and the surface results over the poles are mainly due to errors in the CERES cloud mask during the polar night and at low solar zenith angles (e.g., Spangenberg et al., 2004). Most of the underestimations are due to the presence of very thin clouds that produce little signature for detection. Reliably detecting clouds is extremely difficult in the cold, low thermal contrast conditions of the polar regions using infrared data. During the summer when the visible and near-infrared channels are available, the agreement is much better in the Arctic (not shown). The difficulty is even greater when only one infrared channel (e.g., ISCCP) is used for cloud detection over the Arctic. Outside of the Arctic, it is not clear which datasets better represent the cloud amounts. Many spatial and temporal sampling issues must be taken into account before the differences can be adequately reconciled. For example, the surface and ISCCP observations include samples from all times of day whereas the *Terra* samples during mid morning and before midnight. Over areas with a substantial diurnal cycle, the *Terra* orbit can bias the results. Minnis et al. (2003) found that 0.02-0.11 more cloud cover was found with *Aqua* over land areas at 1330 LT than with *Terra* at 1030 LT, while similar amounts were detected at night. CERES uses a combination of satellites to account for such diurnal effects.

Figure 3 breaks down the cloud cover over ocean by phase. Liquid water clouds (Fig. 3a) are most prevalent in the Northern Hemisphere midlatitudes and polar regions during summer and, conversely, are found least often in the Southern Hemisphere during the same season. The opposite seasonal variation occurs in the Tropics with more liquid water clouds detected in the Northern Hemisphere during summer. The seasonal cycle is due to changing temperature patterns and, in some part, to the variations in ice cloud cover that can block the satellite view of underlying water clouds. For example, the maximum in ice cloud cover coincides with the minimum in liquid water clouds during the Northern Hemisphere winter and vice versa during the summer. Multilayer cloud detection methods and a deeper analysis of surface data would be needed to determine if the liquid cloud cover actually decreases during winter or if it is simply taken out of view by the ice clouds. The water cloud coverage over land (not shown)varies less with season than over water, except in the Arctic. Ice cloud amounts shift latitudinally with season producing a minimum during summer in the Northern Hemisphere and maxima during spring and fall.

The distribution of daytime monthly mean cloud-top heights are plotted in Fig. 4 for January and July 2003. During January, the cloud tops are quite low, on average, over northern Canada and Siberia, possibly as a result of strong inversions or nearly isothermal conditions that make it difficult to place a cloud vertically based on its remotely sensed temperature. Average cloud heights are also below 1 km over small areas off the west coasts of several continents in the sub-tropical high pressure regions. The cloud heights tend to gradually increase to the west from these areas. Mean cloud heights are greatest over North America during

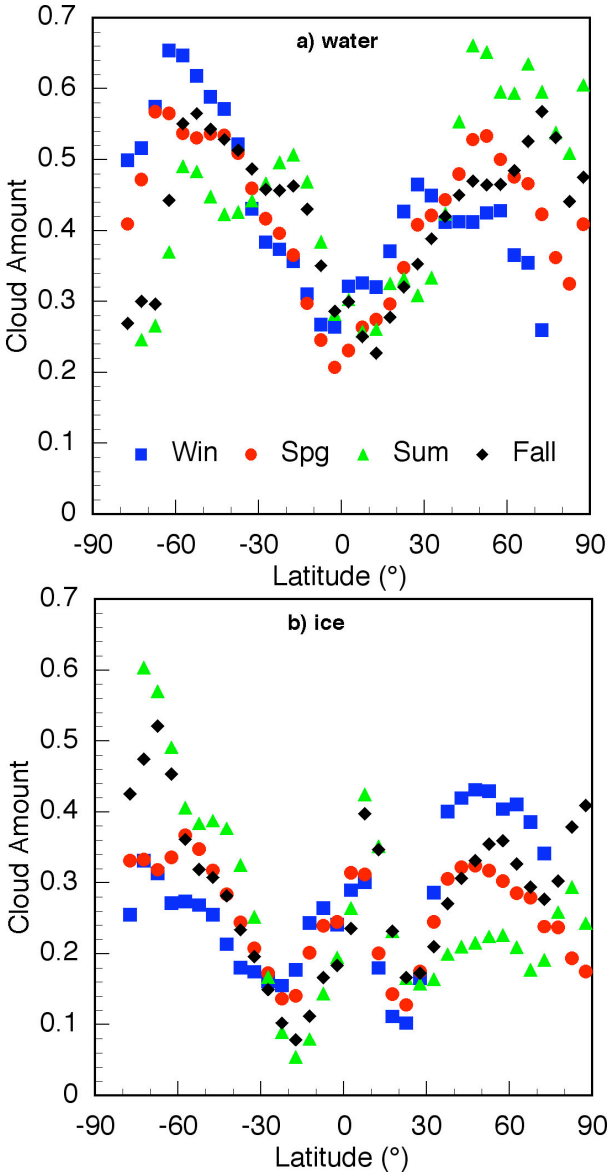


*Fig. 3. Same as Fig. 1, but for liquid water and ice clouds over ocean.*

July and least over South America. Based on the rather high mean altitudes ($z_c$ > 8 km) it appears that most of cloudiness over the Sahara Desert and Saudi Arabian Peninsula appears to be composed of cirrus clouds while the clouds over the eastern Mediterranean Sea are primarily low clouds. The ITCZ appears to be more vigorous during July than January with much of the activity occurring in the South Pacific Convergence Zone. Figure 4 is fairly typical of the average cloud height patterns. The seasonal variations in $z_c$ over land for the period of record (Fig. 5) show the seasonal shift of the ITCZ (Fig. 5b) and increase in the average heights of both water (Fig. 5a) and ice clouds during the summer in the Northern Hemisphere. Zonally, the mean water cloud heights can vary by up to 2 km while the ice cloud mean altitudes can change by more than 3 km.

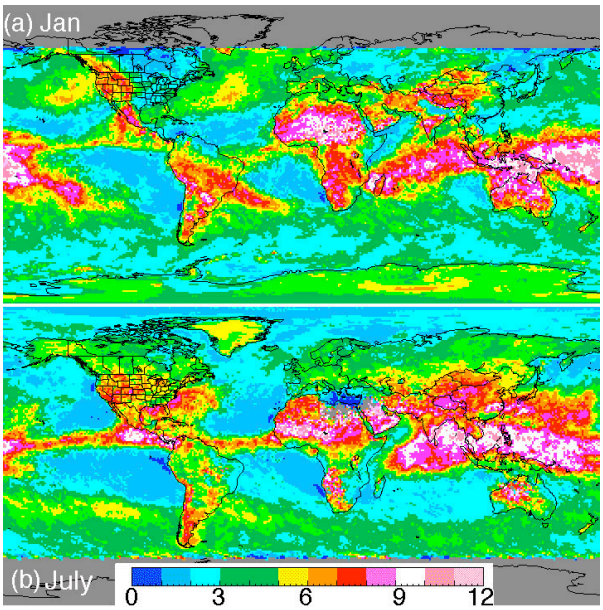


*Fig. 4. Mean cloud-top altitude (km) from CERES Terra data, 2003.*

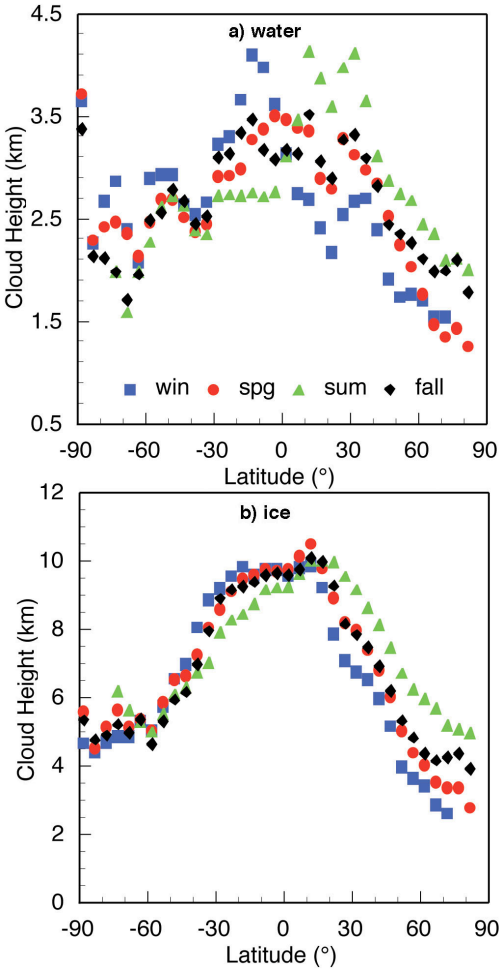


*Fig. 5. Mean seasonal cloud-top heights over land from CERES Terra MODIS, 2000-2003.*

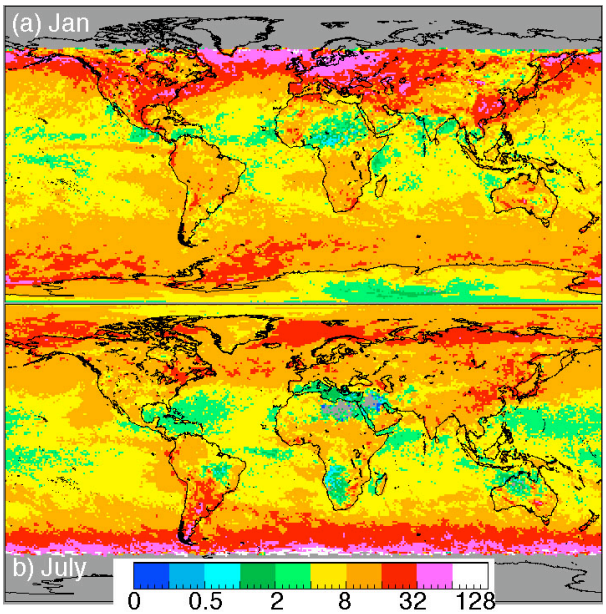


*Fig. 6. Same as Fig. 4, except for mean water cloud optical depth.*

The distributions of linearly averaged liquid cloud optical depth for the 2 example months are shown Fig. 6. The average values for the stratocumulus clouds in the subtropical high areas are around 10, while the trade cumulus cloud *OD* ranges from 3 to 8. The stratus clouds in the Northern Hemisphere (NH) storm tracks during January have the largest optical depths averaging between 16 and 32. The thickest water clouds are found at similar latitudes in the Southern Hemisphere (SH) during July. This seasonal switch in *OD* is more readily seen in Fig. 7, which shows the seasonal variability in water and ice cloud *OD* for ocean areas. Both ice and water clouds show the NH maximum during winter with the opposite variation in the SH. Over land areas (not shown), the maximum mean *OD* occurs during summer north of 50°N and during winter and fall around 30°N, However, the liquid water clouds are thickest over NH land during winter and vice versa in the SH. The decrease in ice *OD* poleward of 50°N over ocean and 40°N over land during winter and spring may be related to the use of the SINT over snow-covered surfaces, but because the method has not been examined in depth yet, it cannot be concluded whether the drop is an artifact or an actual decrease in *OD*. On average, the ice *OD* exceeds the water cloud *OD* because of the influence of deep convective and multilayered clouds on the linear averaging of *OD*. A portion of the large ice cloud *OD* is due to water clouds underneath upper level cirrus clouds. Efforts to separate the ice and liquid water cloud effects in such conditions are continuing (e.g., Huang et al., 2004).

Figure 8 shows the mean cloud water droplet effective radius distribution for January and July 2003 from *Terra*. The values of $r_e$ are smallest over land and desert areas. Over water, $r_e$ is least near coastal areas and greatest over open ocean. During January, strong

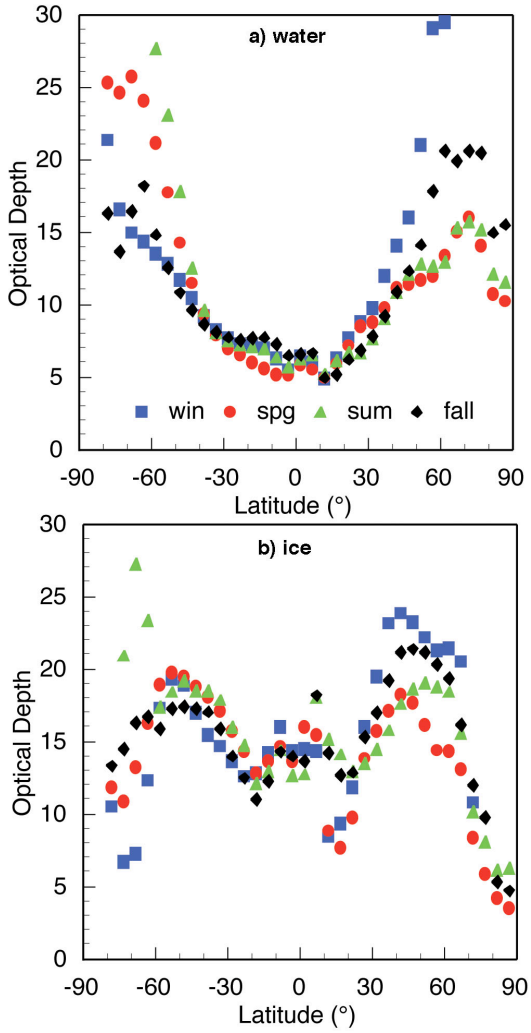


*Fig. 7. Same as Fig. 5, except for cloud OD over water.*

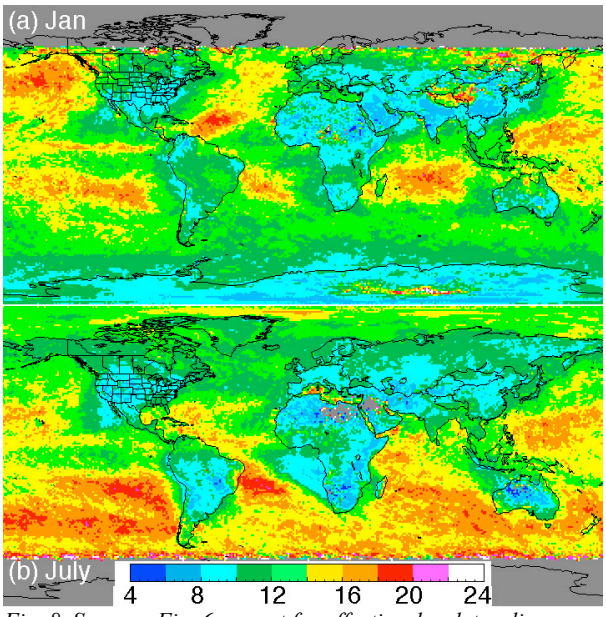


*Fig. 8. Same as Fig. 6, except for effective droplet radius.*

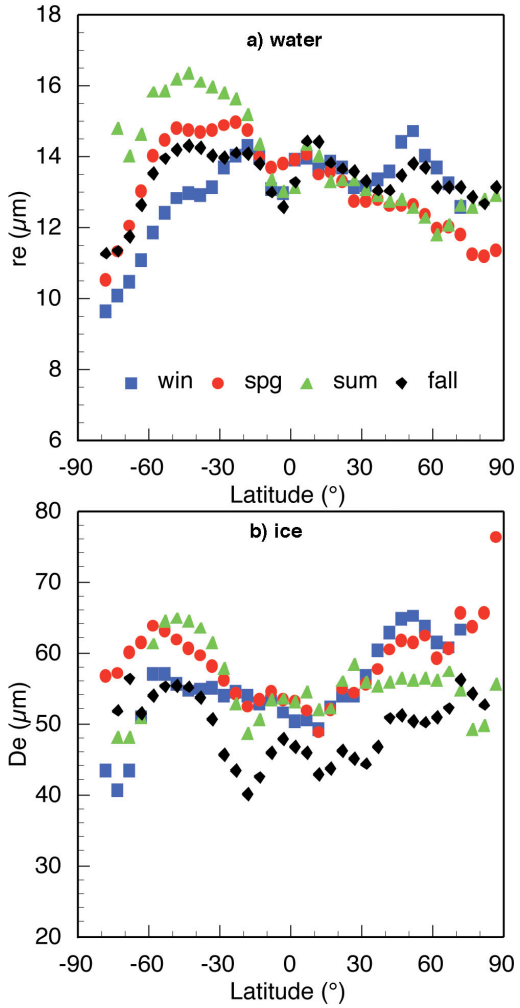


*Fig. 9. Same as Fig. 7, except for effective cloud particle size.*

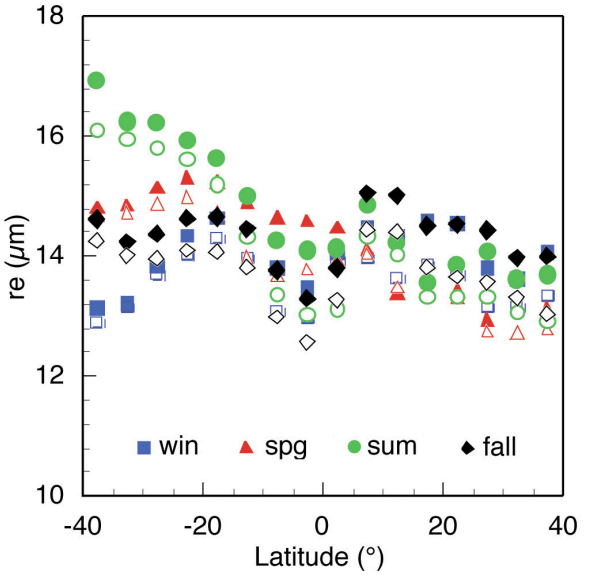


*Fig. 10. Comparison of seasonal variation in $r_e$ ove ocean from Terra MODIS (open), 2000-2003, and VIRS (solid), 1998-2000.*

westerly flow off the North American and Asian coasts is probably responsible for the smaller values of $r_e$ east of those continents while an increase in burning over southern Africa during July may be the source of the decreased $r_e$ over the South Atlantic. Similar burning over South America may also help reduce $r_e$ over Brazil during July. The very large values of $r_e$ over the oceans are probably linked to drizzling clouds in those pristine areas. The even greater values near the terminator lines are likely due to ice contamination or to the effects of lower sun angles and shadowing.

The seasonal variations in $r_e$ and $D_e$ for the study period are plotted in Fig. 9 for ocean areas. These plots include all pixels identified as water clouds and will include some ice cloud contamination whenever the overlying ice cloud is thin enough to yield a water retrieval instead of ice. Maximum values of $r_e$ occur in the SH during the boreal spring and summer. Conversely, the NH minima occur at the same time. The maximum variations are also found in the SH. Similar variability is seen over land (not shown), except that the spring and fall values are very close. Variations in the Tropics are relatively small for $r_e$ over water and $D_e$ over land (not shown). Greater tropical seasonal changes are seen in $D_e$ over water and $r_e$ over land. The mean effective radius changes very little with season, except for winter, over NH land. The mean value of $D_e$ in the Tropics over land is around 45 $\mu$m compared to approximately 51 $\mu$m over water.

The SZA varies seasonally with latitude and might be related to the extreme seasonal variation in $r_e$ over the SH oceans even though preliminary analyses indicate very little dependence of $r_e$ on SZA (Heck et al., 2002). If anything, it decreases slightly with increasing SZA. To ensure that the variability is not due to SZA, the seasonal means in $r_e$ over ocean were computed from the VIRS and *Terra* datasets and plotted in Fig. 10. The VIRS samples all available SZAs for a given zone during a season and should cover the same range of SZA in a given latitude belt in both hemispheres. If the variations are due to angular effects, then the NH and SH should produce the same type of seasonal variability. Figure 10 shows that the VIRS and MODIS data produce similar zonal patterns of mean $r_e$ and that the extreme variation in $r_e$ over the SH is probably due to some other effect, which is probably related to the availability of more cloud condensation nuclei during the austral summer. Determining why this variability occurs should greatly advance our understanding of cloud processes and the natural production of aerosols.

Although many more parameters could be examined, a complete analysis of the CERES cloud dataset is beyond the scope of this paper. Table 1 summarizes the mean values of the quantities considered here from CERES's analysis of the *Terra* MODIS data for 2000 - 2003 for the zone between 75°N and 75°S to ensure equal sampling. Over oceans, liquid water clouds cover 64% more area than ice clouds, while over land, coverage by the two phases is nearly

*Table 1. Mean cloud properties from CERES using daytime Terra MODIS data, 2000-2003, 75°S - 75°S.*

| parameter | ocean | | land | |
|---|---|---|---|---|
| | water | ice | water | ice |
| Ac (%) | 41.0 | 25.0 | 25.9 | 26.9 |
| z (km) | 2.10 | 7.35 | 2.81 | 7.44 |
| OD | 11.5 | 16.1 | 13.9 | 14.7 |
| Re / De ($\mu$m) | 13.7 | 56.4 | 11.3 | 50.2 |

the same. Water clouds tend to be higher over land because of the surface elevations, but the average heights of the ice clouds are almost identical. The water cloud *OD*s are greater over land, while the ice clouds tend to be slightly thicker over ocean. The mean cloud particle sizes are significantly smaller over land than ocean regardless of phase. These results suggest that the ice particles are affected by the enhanced aerosols over land in a fashion similar to that for liquid water clouds. Whether this is the result of more vigorous convective activity over land, which could inject more small frozen droplets into the upper troposphere or due to aerosols requires further study.

The mean cloud properties between 60°N and 60°S were computed for each year to determine the interannual variations. The average cloud heights, fractional coverage and optical depths are essentially invariant over the 4 years, a result that precludes clouds as the mechanism for an apparent increase in the Earth's albedo estimated from lunar measurements (Palle et al., 2004).

## 4. CONCLUDING REMARKS

This paper has presented a brief summary of the first 4 years of cloud properties derived from *Terra* MODIS data for CERES. Despite known shortcomings in the cloud retrieval process, the results are consistent between satellites and with surface measurements, in general. Much more validation work remains but the data are already proving valuable for radiation budget studies and should be especially useful for studying cloud and aerosol interactions and performing climate model validations. The data are publicly available at the NASA Langley Research Center Distributed Active Archive. Additional data from *Terra* and *Aqua* will be archived as data processing continues.

**ACKNOWLEDGEMENTS**

This research was supported by the NASA Earth Science Enterprise through the CERES Project.

## REFERENCES

Arduini, R. F., P. Minnis, and D. F. Young, 2002: Investigation of a visible reflectance parameterization for determining cloud properties in multi-layered clouds. *Proc. 11th AMS Conf. Cloud Physics.*, Ogden, UT, June 3-7, CD-ROM, P2.4.

Chen, Y., S. Sun-Mack, P. Minnis, D. F. Young, and W. L. Smith, Jr., 2002: Surface spectral emissivity derived from MODIS data. *Proc. SPIE 3rd Intl. Asia-Pacific Environ. Remote Sensing Symp.: Remote Sens. of Atmos., Ocean, Environment, and Space*, Hangzhou, China, October 23-27, **4891**, 361-369.

DAO, 1997: GEOS-3 Data Assimilation System Architectural Design. *DAO Office Note 97-06*. Data Assimilation Office, Goddard Space Flight Center, Greenbelt, MD 20771.

Hahn, C. J., and S. G. Warren, 1999: *Extended Edited Synoptic Cloud Reports from Ships and Land Stations Over the Globe, 1952-1996.* NDP026C, Carbon Dioxide Information Analysis Center, Oak Ridge National Laboratory, Oak Ridge, TN.

Heck, P. W., P. Minnis, D. F. Young, and S. Sun-Mack, 2002: Angular variations of cloud properties from VIRS and MODIS data. *Proc. 11th AMS Conf. Atmos. Rad.*, Ogden, UT, June 3-7, 148-151.

Huang, J., P. Minnis, B. Lin, Y. Yi, M. M. Khaiyer, R. F. Arduini, and G. G. Mace, 2004: Advanced retrievals of multilayered cloud properties using multi-sensor and multi-spectral measurements. Accepted, *J. Geophys. Res.*, 10.1029/2004JD005101.

Loeb, N. G., N. Manalo-Smith, S. Kato, W. F. Miller, S. Gupta, P. Minnis, and B. A. Wielicki, 2003: Angular distribution models for top-of-atmosphere radiative flux estimation from the Clouds and the Earth's Radiant Energy System instrument on the Tropical Rainfall Measuring Mission satellite. Part I: Methodology. *J. Appl. Meteorol.*, **42**, 240-265.

Minnis, P., D. P. Garber, D. F. Young, R. F. Arduini, and Y. Takano, 1998: Parameterization of reflectance and effective emittance for satellite remote sensing of cloud properties. *J. Atmos. Sci.*, **55**, 3313-3339.

Minnis, P., et al., 1995: Cloud Optical Property Retrieval (Subsystem 4.3). "Clouds and the Earth's Radiant Energy System (CERES) Algorithm Theoretical Basis Document, Volume III: Cloud Analyses and Radiance Inversions (Subsystem 4)", *NASA RP 1376 Vol. 3*, pp. 135-176.

Minnis, P., D. F. Young, S. Sun-Mack, P. W. Heck, D. R. Doelling, and Q. Z. Trepte, 2003: CERES cloud property retrievals from imagers on TRMM, Terra, and Aqua. *SPIE 10th Intl. Symp Remote Sens., Conf. Remote Sens. Clouds and Atmos.*, Barcelona, Spain, September 8-12, 37-48.

Minnis, P., D. F. Young, B. A. Weilicki, S. Sun-Mack, Q. Z. Trepte, Y. Chen, P. W. Heck, and X. Dong, 2002: A global cloud database from VIRS and MODIS for CERES. *Proc. SPIE 3rd Intl. Asia-Pacific Environ. Remote Sensing Symp. 2002: Remote Sens. of Atmosphere, Ocean, Environment, and Space*, Hangzhou, China, October 23-27, Vol. 4891, 115-126.

Pallé, E., P. R. Goode, P. Montañés-Rodríguez, and S. E. Koonin, 2004: Changes in Earth's reflectance over the past two decades. *Science*, **304**, 1299-1301

Platnick, S., J. Y. Li, M. D. King, H. Gerber, and P. V. Hobbs, A solar reflectance method for retrieving cloud optical thickness and droplet size over snow and ice surfaces. *J. Geophys. Res.*, **106**, 15185-15199, 2001.

Rossow, W. B. and R. A. Schiffer, 1999: Advances in understanding clouds from ISCCP. *Bull Am. Meteor. Soc.*, **80**, 2261-2287.

Spangenberg, D. A., Q. Trepte, P. Minnis, and T. Uttal, 2004: Daytime cloud property retrievals over the Arctic from multispectral MODIS data. *Proc. 13th AMS Conf. Satellite Oceanogr. and Meteorol.*, Norfolk, VA, Sept. 20-24, CD-ROM, P7.11.

Sun-Mack, S., Y. Chen, T. D. Murray, P. Minnis, and D. F. Young, 1999: Visible clear-sky and near-infrared surface albedos derived from VIRS for CERES. *Proc. AMS 10th Conf. Atmos. Rad.*, Madison, WI, June 28 – July 2, 422-425.

Sun-Mack, S., P. Minnis, Y. Chen, and R. F. Arduini, 2003: Clear-sky narrowband albedos derived from VIRS and MODIS. *SPIE 10th Intl. Symp Remote Sens., Conf. Remote Sens. Clouds and Atmos.*, Barcelona, Spain, September 8-12, 101-109.

Trepte, Q., Y. Chen, S. Sun-Mack, P. Minnis, D. F. Young, B. A. Baum, and P. W. Heck, 1999: Scene identification for the CERES cloud analysis subsystem. *Proc. AMS 10th Conf. Atmos. Rad.*, Madison, WI, June 28 – July 2, 169-172.

Trepte, Q., P. Minnis, and R. F. Arduini, 2002: Daytime and nighttime polar cloud and snow identification using MODIS data. *Proc. SPIE 3rd Intl. Asia-Pacific Environ. Remote Sensing Symp. 2002: Remote Sens. of Atmosphere, Ocean, Environment, and Space*, Hangzhou, China, October 23-27, Vol. 4891, 449-459.

Wielicki, B. A., et al., 1998: Clouds and the Earth's Radiant Energy System (CERES): Algorithm overview. *IEEE Trans. Geosci. Remote Sens.*, **36**, 1127-1141.